Reduction of staircase effect with total generalized variation regularization for electrical impedance tomography

Yanyan Shi, Xu Zhang, Zuguang Rao, Meng Wang and Manuchehr Soleimani

***Abstract*—Image reconstruction in electrical impedance tomography is an ill-posed inverse problem. To address this problem, regularization methods such as Tikhonov regularization and total variation regularization have been adopted. However, the image is over-smoothed when reconstructing with the Tikhonov regularization and staircase effect appears in the image when using the total variation regularization. In this paper, total generalized variation regularization method which combines the first-order and the second-order derivative terms to perform as the regularization term is proposed to cope with the above problems. The weight between the two derivative terms is adjusted by the weighting factors. Chambolle-Pock primal-dual algorithm, an efficient iterative algorithm to handle optimization problem and solve dual problem, is developed. Simulation and experiments are performed to verify the performance of the total generalized variation regularization method against other regularization methods. Besides, relative error and correlation coefficient are also calculated to estimate the proposed regularization methods quantitatively. The results indicate that the staircase effect is effectively reduced and the sharp edge is well preserved in the reconstructed image.**

***Index Terms*—Electrical impedance tomography, image reconstruction, staircase effect, total generalized variation.**

I. INTRODUCTION

ELECTRICAL impedance tomography (EIT) is a visualization and measurement technique designed to reconstruct the complex conductivity distribution of the detected area [1], [2]. It is realized by injecting current and measuring the voltage data on its boundary [3]. Due to its advantages of safety, low cost, high speed, non-invasion and non-radiation, EIT is widely applied in industrial process imaging, nondestructive testing of materials, geophysical exploration and biomedical imaging [4]-[7]. In the biomedical application, it has shown great potential in the thorax imaging, lung ventilation monitoring, tumor detecting and brain function [8]-[15]. The conductivity of the biological tissues can be reconstructed from the measured voltage.

However, the recovering of an unknown conductivity distribution from boundary voltage data is a severely ill-posed inverse problem, which hinders the application of EIT [16], [17]. Usually, the number of the independent measured data is much fewer than that of the unknown conductivity, leading to an inevitable under-determined problem. In addition, a small disturbance of noise to the boundary voltage will exert a great influence on the calculated conductivity distribution. To solve the ill-posed inverse problem, a variety of regularization methods with a regularization term added to the objective function has been presented to stabilize the solution [18]-[20]. Among these methods, Tikhonov regularization is commonly used as it stabilizes the solution. However, as a regularization method of L_2-norm, Tikhonov regularization makes the edges of reconstructed image over-smoothed and results in an image with low sharpness [21], [22]. To solve this problem, total variation (TV) regularization is proposed with the L_1-norm as the regularization term. It prevents the edges from being over-smoothed and the sharp edge of the reconstructed image is preserved [23], [24]. Nevertheless, unwanted staircase effect is produced with TV regularization method [25]. To overcome the problem of staircase effect, a variety of improved TV regularization methods have been presented. In [26], in order to solve the problem of staircase effect in the image of cone-beam computed tomography, a new family of Hessian Schatten penalties is proposed. In [27], a nonlocal TV regularization associated with the quadratic perturbation of a regularization functional model is studied to restrain the staircase effect in the recovered image. In [28], two detection operators are proposed to solve the staircase effect problem and an adaptive image denoising TV model is proposed. In [29], an improved TV regularization is proposed based on a denoising model by using an edge detection function to inhibit the staircase effect and remove mixed noise. The methods mentioned above are all based on the TV method. Due to the inherent defect of TV, the stair effect is merely reduced to a certain extent. Total generalized variation (TGV) regularization method is firstly proposed in [30]. It is an effective method to approximate a polynomial function with arbitrary order. Up until now, the applications of TGV are mostly concentrated on image processing. In [31], a new color transfer model based on adaptive TGV regularization is presented to address the staircase effect and the image detail in the synthetic images is well preserved. In [32], a TGV model is established to remove the multiplicative noise and overcome the staircase effect. In this paper, the TGV regularization method is investigated for image reconstruction in EIT and an efficient Chambolle-Pock primal-dual algorithm is developed to solve the proposed regularization method.

This paper is organized as follows: In Section II, the mathematical model of the EIT is presented. In Section III, two typical regularization methods, Tikhonov and TV, are introduced for comparison. In Section IV, the TGV regularization method is proposed for image reconstruction of

Manuscript received ××××, ××××; revised ××××, ××××; accepted ××××, ××××. This work was supported in part by the National Natural Science Foundation of China under Grant 61640303 and in part by the Science Foundation for the Excellent Youth Scholars of Henan Normal University under Grant 2017GGJS040. (*Corresponding author: Meng Wang*.)

Y. Shi, X. Zhang, M. Wang and Z. Rao are with the Department of Electronic and Electrical Engineering, Henan Normal University, Xinxiang 453007, China.

M. Soleimani is with the Department of Electronic and Electrical Engineering, University of Bath, Bath BA2 7AY, UK.

EIT which is solved by the Chambolle-Pock primal-dual algorithm. In Section V, the simulation and experiments are performed to validate the performance of the TGV regularization method in reducing staircase effect and preserving the sharp edge in the reconstructed image. Finally, Section VI provides the conclusions.

II. Mathematical Model of EIT

Generally, a complete EIT system is comprised of three main parts: an array of sensors, a data acquisition system and a computer used for image reconstruction. A typical EIT sensor array is illustrated in Fig. 1 which consists of sixteen electrodes. The electrodes are attached on the external surface of detected object. The current is injected into two adjacent electrodes and then the resulting voltage is measured from the adjacent electrodes [33]. Finally, the internal conductivity distribution is reconstructed from the measured data.

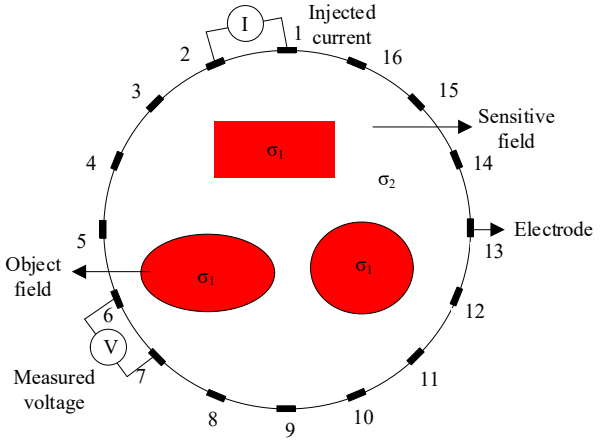

Fig. 1. Operating principle of EIT.

Based on Maxwell's electromagnetic field theory, the sensitive field of the EIT system can be expressed as:

$$\begin{aligned} D &= \sigma E \\ \nabla \cdot D &= 0 \\ E &= -\nabla \varphi \end{aligned} \tag{1}$$

where D is the current density vector, σ is the conductivity, E is the electric field and φ is the potential distribution.

Based on (1), it can be obtained as:

$$\nabla \cdot (\sigma \cdot \nabla \varphi) = 0 \tag{2}$$

The relationship between the boundary voltage and the conductivity distribution is nonlinear and can be expressed as:

$$u = f(\sigma) \tag{3}$$

where u is the boundary voltage.

For conductivity distribution with small variation, (3) can be solved by simplifying the variation of the boundary voltage to a linear form as:

$$\Delta u = \frac{\mathrm{d}f(\sigma)}{\mathrm{d}\sigma} \cdot \Delta\sigma \tag{4}$$

where $\Delta\sigma$ is the perturbation of the conductivity distribution, Δu is the variation of the boundary voltage caused by the change of the conductivity.

The linearized and normalized form of (4) is derived as [34]:

$$b = Ag \tag{5}$$

where $b \in R^{m\times 1}$ represents the change of the measured boundary voltage, $A \in R^{m\times n}$ is the Jacobian matrix denoting the sensitivity of the boundary voltage to the change of conductivity and can be calculated based on Geselowitz's sensitivity theorem, $g \in R^{n\times 1}$ is the difference of conductivity distribution in the reconstructed field, m is the number of measurement and n is the number of pixels of the reconstructed image.

III. Regularization Methods

For EIT, the objective of image reconstruction is to obtain the unknown conductivity distribution from the known measured boundary voltage. It is typically an ill-posed inverse problem. Generally, regularization methods are effective in dealing with such problem, which improves the stability of the solution by adding a regularization term to the least squares problem. The general form of the regularization method can be expressed as:

$$F(g) = \frac{1}{2}\|Ag - b\|_2^2 + \lambda R(g) \tag{6}$$

Where λ is the regularization parameter which controls the tradeoff between the fidelity term $\|Ag - b\|_2^2$ and the regularization term $R(g)$.

Theoretically, the optimal solution can be found when $F(g)$ is minimized. Among the regularization methods, Tikhonov regularization method has been widely used to solve the ill-posed problem. The standard form of the Tikhonov regularization method for EIT can be described as:

$$F(g) = \frac{1}{2}\|Ag - b\|_2^2 + \lambda \|g\|_2^2 \tag{7}$$

The Tikhonov algorithm is stable and performs well for image reconstruction of continuous conductivity distribution. However, excessive smoothness is imposed on the edge of image as the regularization term is L_2-norm. As a result, the image quality of the reconstructed image is poor.

To preserve the sharp discontinuous edge, the TV regularization method is proposed and can be represented as:

$$F(g) = \frac{1}{2}\|Ag - b\|_2^2 + \lambda \int_\Omega |\nabla g| \mathrm{d}x \tag{8}$$

The TV regularization method is based on the regularization term with L_1-norm which is advantageous for edge retention. However, staircase effect is induced in the smooth region of the reconstructed image as piecewise constant function is reconstructed.

For further improvement of image quality in EIT, an image reconstruction method based on the TGV regularization is investigated to address the staircase effect in this work.

IV. TGV Regularization Method

A. TGV Regularization Method for EIT

The TGV regularization is a generalization form of the TV regularization [35]. For TGV regularization with the order $k \geq 1$ and the positive weights $\alpha = (\alpha_0, \alpha_1, ..., \alpha_{k-1})$, it can be expressed as:

$$\mathrm{TGV}_{\alpha}^{k}(f) = \sup\left\{\int_{\Omega} f \,\mathrm{div}^{k} v \mathrm{d}x\right\} \tag{9}$$

where

$$v \in C_c^k(\Omega, \mathrm{Sym}^k(\mathbb{R}^2)) \text{ and } \| \mathrm{div}^l v \|_{\infty} \leq \alpha_l, l = 0, ..., k-1 \tag{10}$$

and where f is the image function, Ω is the image domain and $\Omega \subset \mathbb{R}^2$, $C_c^k(\Omega, \mathrm{Sym}^k(\mathbb{R}^2))$ is the space of compactly supported symmetric k-tensor fields, $\|.\|_{\infty}$ is the L^{∞} norm, $\mathrm{Sym}^k(\mathbb{R}^2)$ is the symmetric tensor space with the kth order.

When k is 1 and α is 1, (9) is converted to TV regularization, i.e. $\mathrm{TGV}_1^1(f) = \mathrm{TV}(f)$. When k is 2, the second-order TGV is defined as [36]:

$$\mathrm{TGV}_{\alpha}^{2}(f) = \sup\left\{\int_{\Omega} f \,\mathrm{div}^{2} v \mathrm{d}x\right\} \tag{11}$$

where

$$v \in C_c^2\left(\Omega, \mathrm{Sym}^k\left(\mathbb{R}^2\right)\right), \| v \|_{\infty} \leq \alpha_0, \| \mathrm{div} v \|_{\infty} \leq \alpha_1 \tag{12}$$

Equation (11) can be also written as:

$$\mathrm{TGV}_{\alpha}^{2}(f) = \alpha_1 \int_{\Omega} |\nabla f - v| \mathrm{d}x + \alpha_0 \int_{\Omega} |\varepsilon(v)| \mathrm{d}x \tag{13}$$

where α_1 and α_0 are used to weigh the first and second derivatives of the second-order TGV regularization function

Based on the Legendre-Fincher transform, the second-order TGV is rewritten in L_1- norm as:

$$\mathrm{TGV}_{\alpha}^{2}(f) = \alpha_1 \left\| \nabla f - v \right\|_1 + \alpha_0 \left\| \varepsilon(v) \right\|_1 \tag{14}$$

where $\varepsilon(v) = \left(\nabla v + \nabla v^{\mathrm{T}}\right)/2$ denotes a symmetrized gradient operator.

It can be observed from (14) that the weights α_1 and α_0 establish the tradeoff between the discontinuous and smooth solutions. Compared with the TV regularization method which reconstructs the piecewise constant function, the TGV shows advantages in reconstructing piecewise polynomial function. As a result, the staircase effect appearing in the TV regularization may be reduced [37], [38].

In this paper, the second-order TGV regularization method is investigated for the image reconstruction in EIT. Equation (6) is then described as:

$$\begin{aligned} F(g) &= \frac{\lambda}{2} \| Ag - b \|_2^2 + \mathrm{TGV}(g) \\ &= \frac{\lambda}{2} \| Ag - b \|_2^2 + \alpha_1 \left\| \nabla g - v \right\|_1 + \alpha_0 \left\| \varepsilon(v) \right\|_1 \end{aligned} \tag{15}$$

In the image reconstruction of EIT, the objective function is expressed as a regularized least square minimization:

$$\bar{g} = \arg\min_{g} F(g) \tag{16}$$

B. Chambolle-Pock Primal-Dual Algorithm

According to the Legendre-Fenchel duality, the dual form of (16) can be derived as:

$$\min_{u,v} \max_{p \in P, q \in Q} \langle \nabla u - v, p \rangle + \langle \varepsilon(v), q \rangle + \frac{\lambda}{2} \| Ag - b \|_2^2 \tag{17}$$

where

$$P = \left\{ p = (p_1, p_2) \middle| \left\| p \right\|_{\infty} \leq \alpha_1 \right\} \tag{18}$$

$$Q = \left\{ q = \begin{pmatrix} q_{11}, q_{12} \\ q_{21}, q_{22} \end{pmatrix} \middle| \left\| q \right\|_{\infty} \leq \alpha_0 \right\} \tag{19}$$

To solve the minimization problem in (17), the Chambolle-Pock primal-dual algorithm which deals with optimization along with its dual is studied [39], [40]. In this work, the Chambolle-Pock primal-dual algorithm for TGV regularization in EIT image reconstruction is written in Algorithm 1.

Algorithm 1 Chambolle-Pock primal-dual algorithm for TGV regularization

Initialize: Set $w, v, \bar{v}, p, \bar{p}, q$,and g_0 are to zeros values.

Given constant λ and L. Let $\tau = 1/L, \sigma = 1/L$

For k = 0, 1, 2, ⋯ do

1. $p^{k+1} = \mathrm{proj}_P(p^k + \sigma(\nabla \bar{p}^k - \bar{v}^k))$
2. $q^{k+1} = \mathrm{proj}_Q(q^k + \sigma(\varepsilon(\bar{v}^k)))$
3. $w^{k+1} = \mathrm{prox}^{\sigma}(w^k + \sigma(A\bar{g}^k - b))$
4. $g^{k+1} = g^k + \tau(\mathrm{div} \nabla p^{k+1} - \mathrm{A}^{\mathrm{T}} w^{k+1})$
5. $v^{k+1} = v^k + \tau(p^{k+1} + \mathrm{div} \varepsilon q^{k+1})$
6. $\bar{g}^{k+1} = 2g^{k+1} - g^k$
7. $\bar{v}^{k+1} = 2v^{k+1} - v^k$

end do

In Algorithm 1, $\mathrm{div}\varepsilon$ represents the negative conjugate of symmetric gradient operator ε, that is, $\mathrm{div}\varepsilon = -\varepsilon$. The proximal mappings onto convex sets P and Q are given by:

$$\mathrm{proj}_P(\bar{p}) = \frac{\bar{p}}{\max(\lambda, \frac{\lambda |\bar{p}|}{\alpha_1})} \tag{20}$$

$$\mathrm{proj}_Q(\bar{q}) = \frac{\bar{q}}{\max(\lambda, \frac{\lambda |\bar{q}|}{\alpha_0})} \tag{21}$$

V. Results and Discussions

In this section, the performance of the proposed TGV regularization method in the image reconstruction of the EIT is investigated with numerical simulation and experimental work.

A. Simulation and Discussions

All the simulations are performed with MATLAB2016a installed on a computer environment with Intel Core 2 multiple CPUs of 2.3 GHz. EIDORS is used in the construction of the forward model which is solved based on finite element method (FEM). A complete boundary condition is applied for current injection. The triangular mesh is adopted in the forward problem while the square mesh is employed in the inverse solution to display the sharp edge of the detected object, as shown in Fig. 2. To avoid inverse crime, the number of elements in the inverse problem is smaller than that in the forward problem. The conductivity of inclusion and background are set as 2 S/m and 1 S/m, respectively. Six models, named as model (a) to model (f), are simulated as shown in Fig. 3.

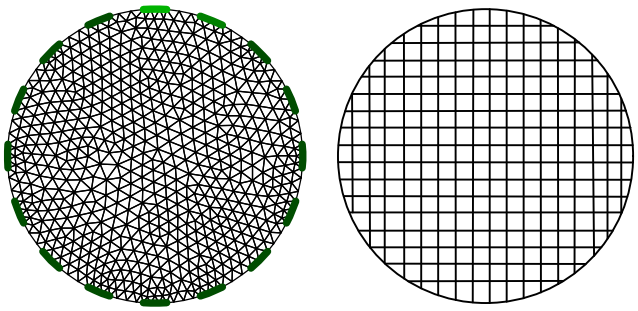

Fig. 2. Meshes for forward and inverse problems: (a) is the triangular mesh in the forward problem; (b) is the square mesh in the inverse problem.

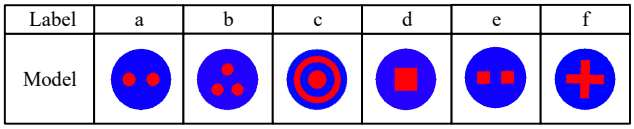

Fig. 3. Six different models in the simulation.

In the regularization methods, the regularization factor is an essential parameter for image reconstruction which controls the weight between the fidelity term and the regularization term. When the regularization factor is too small, the noise can not be well suppressed and serious interference is induced on the image. Nevertheless, the detailed information is lost for a large regularization factor. To determine the regularization factor, several methods have been proposed such as discrepancy principle, generalized cross-validation and L-curve methods. Nevertheless, there is limitation for each method. Prior information of the noise in the measurement is required for the discrepancy principle method. Although less prior information is needed for the other two methods, the related calculations are complicated. As a result, the empirical method has been applied in this work to determine the regularization parameter by repetitive test of image reconstruction until satisfactory reconstructed results are obtained. In this work, the regularization parameters are $\lambda=5\times10^{-2}$ for Tikhonov, $\lambda=1\times10^{-2}$ for TV and $\lambda=1\times10^{-6}$ for TGV respectively. In the TGV model, weighting factors are significant in the establishment of piecewise smooth reconstruction with high quality. As a result, apart from the regularization parameter, weighting factors are also required in the TGV regularization method which is different from the Tikhonov and TV methods.

Fig. 4 shows the reconstructed images obtained by the Tikhonov, TV and TGV regularization methods under noiseless condition. In the image reconstruction, the conductivity of the inclusion and the background is normalized to 1 and 0 respectively. Besides, two different categories of models, models with smooth edges (e.g. model (a)-(c)) and models with sharp edges (e.g. model (d)-(f)), are investigated for comparative analysis. Weighting factors are set to $\alpha_1=10$, $\alpha_0=0.01$ and $\alpha_1=2.5$, $\alpha_0=0.1$ for the models with smooth edges and models with sharp edges, respectively. It can be observed that the reconstructed image with the Tikhonov regularization method has the worst quality and excessive smoothness appears at the image edges. Compared with the Tikhonov regularization method, the quality of the image reconstructed by the TV regularization method is largely improved and the edge is better preserved. However, the reconstructed images of the model (a) and model (b) tend to be square. In addition, the staircase effect is obvious in the recovered image of all models. In comparison to the TV method, the staircase effect is effectively reduced with the proposed TGV regularization method. Besides, excessive smoothness appeared in the Tikhonov method is avoided.

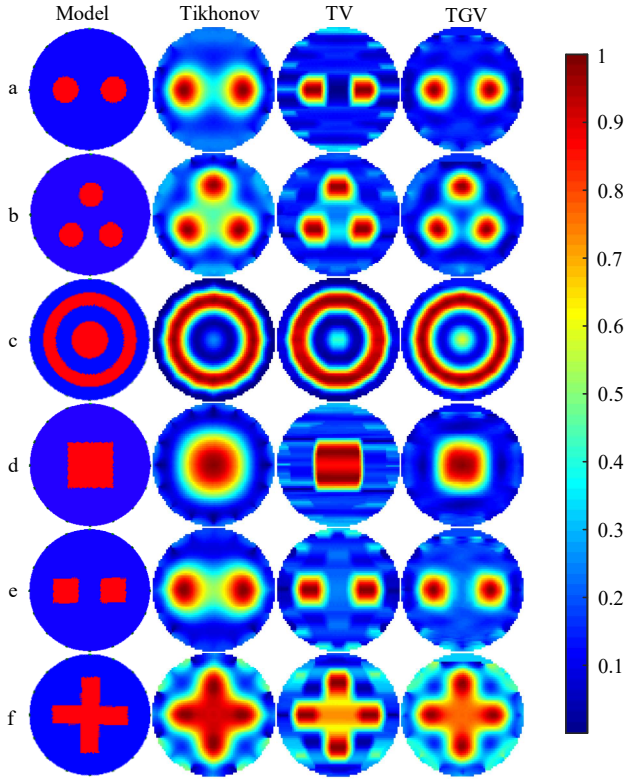

Fig. 4. Image reconstruction without noise.

In order to further evaluate the performance of the algorithms, relative error (RE) and correlation coefficient (CC) are used to determine the reconstructed image quantitatively, which are defined as:

$$\mathrm{RE} = \frac{\left\|\sigma - \sigma^*\right\|_2^2}{\left\|\sigma^*\right\|_2^2} \tag{22}$$

$$\mathrm{CC} = \frac{\sum_{i=1}^{t}\left(\sigma_i - \bar{\sigma}\right)\left(\sigma_i^* - \bar{\sigma}^*\right)}{\sqrt{\sum_{i=1}^{t}\left(\sigma_i - \bar{\sigma}\right)^2 \sum_{i=1}^{t}\left(\sigma_i^* - \bar{\sigma}^*\right)^2}} \tag{23}$$

where σ is the calculated conductivity, σ^* is the real conductivity, σ_i and σ_i^* are the ith elements of σ and σ^*, $\bar{\sigma}$ and $\bar{\sigma}^*$ represent the average values of σ and σ^*.

The RE and CC values of the reconstructed images acquired with the three regularization methods are shown in Fig. 5. As illustrated in Fig. 5, compared with Tikhonov and TV, the RE values are the smallest and the CC values are the largest for the models with smooth edges (model (a)-(c)) when using the proposed TGV regularization method which indicates high quality of image reconstruction as shown in Fig. 4. However, the RE and CC values for models with sharp edges (model (d)-(f)) calculated by the TGV regularization method are almost the same with the TV. The reasons are as follows. For model (a)-(c) with smooth edges, only the staircase effect should be considered which results in the high image quality. For model (d)-(f), both of the reduction of the staircase effect and the preservation of the sharp edge should be considered. As a result, the performance of edge retention in TGV regularization method may be slightly worse than that of TV.

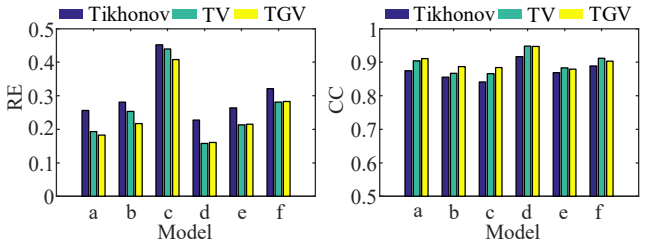

Fig. 5. The RE and the CC of the reconstructed images without noise. (a) The RE values. (b) The CC values.

The real-time performance is one of the key elements to evaluate the reconstruction algorithms in the application of tomography techniques [41]-[44]. TABLE I compares the calculation time of the six simulation models when using the three regularization methods. It can be observed that the calculation time of the proposed TGV regularization method is a bit longer compared with the Tikhonov and TV methods. However, the calculation time is acceptable due to its advantages in reducing staircase effect and avoiding excessive smoothness.

TABLE I
THE CALCULATION TIME OF THE THREE REGULARIZATION METHODS.

Method	Time/s					
	Model (a)	Model (b)	Model (c)	Model (d)	Model (e)	Model (f)
Tikhonov	1.1063	1.0735	1.0719	1.0938	1.0455	1.0846
TV	1.5828	1.6016	1.5609	1.5796	1.6634	1.6568
TGV	1.7777	1.8125	1.7735	1.8082	1.8551	1.8267

In practical application, the interference caused by noise is inevitable. In order to test the anti-noise performance of the three regularization methods, 5% and 10% random noise are added to the measured voltage in the simulation. The measured voltage when the noise is added, U_{noise}, can be expressed as:

$$U_{\mathrm{noise}} = U \cdot (1 + \eta \cdot \mathrm{random} \cdot \bar{U}) \tag{24}$$

where U is the voltage without noise, η is the noise level, $\bar{U}$ is the mean value of U, random is a random vector with values on the open interval (0, 1) and random $\in R^{m\times 1}$.

Fig. 6 shows the simulation results with 5% noise level. It can be noticed that slight deformation appears when compared with the noiseless condition. However, with the proposed TGV method, clearer edge is observed when compared with the Tikhonov method and staircase effect is reduced when compared with the TV method.

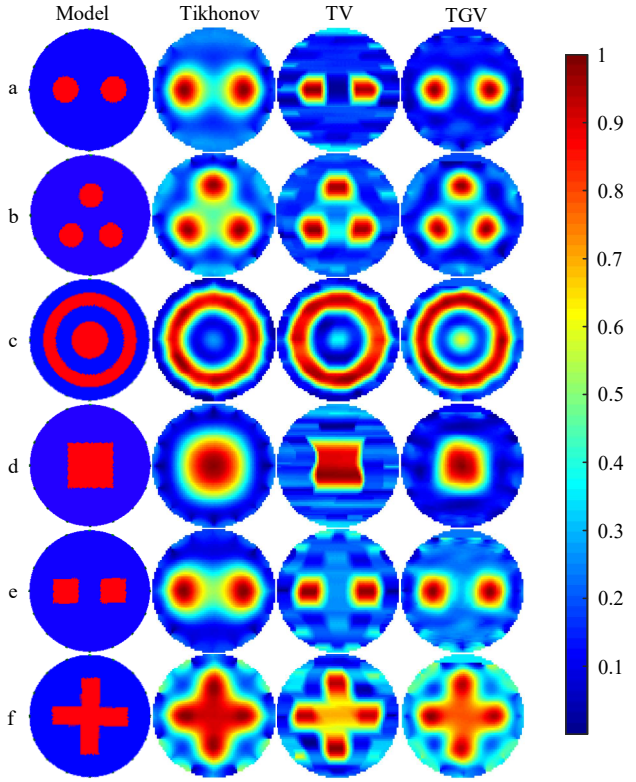

Fig. 6. Image reconstruction with 5% noise level.

The RE and CC values calculated with the three regularization methods under 5% noise level are shown in Fig. 7. Due to the inference of noise, the RE values become larger and the CC values get smaller compared with noiseless condition in Fig. 5. In comparison to the Tikhonov and TV methods, the smallest RE value and the largest CC value are obtained when using the TGV regularization method, which validate the performance of the proposed method in case of noise.

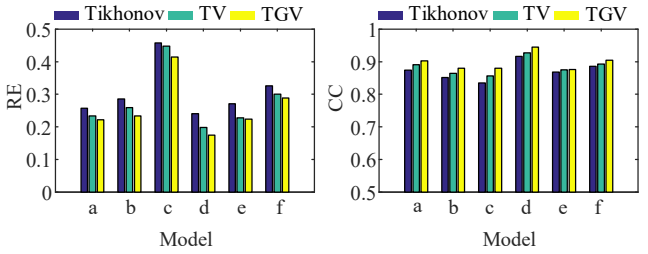

(a) (b)

Fig. 7. The RE and the CC of the reconstructed images with 5% noise level. (a) The RE values. (b) The CC values.

In order to further study the effect of noise on the quality of reconstructed images, 10% noise level is added to the simulated voltage. Under the interference of strong noise, the images reconstructed by the three regularization methods show obvious deformation, as shown in Fig. 8. Nevertheless, the images recovered by the TGV have the most excellent quality and the staircase effect appeared in the TV is inhibited.

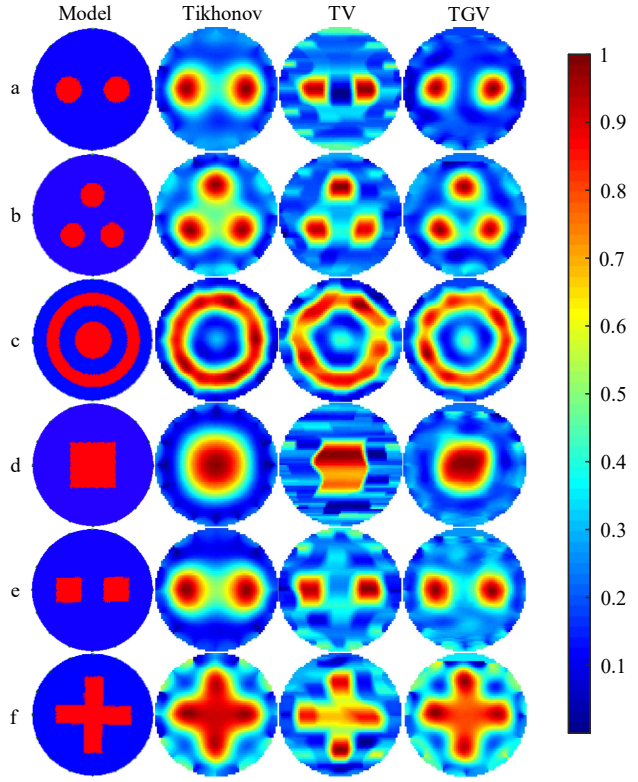

Fig. 8. Image reconstruction with 10% noise level.

To qualitatively estimate the impact of the 10% noise level on the reconstructed images, the RE values and CC values are computed and depicted in Fig. 9. It can be observed that RE values are higher and the CC values are smaller compared with those in Fig. 7 which indicates further deterioration of the reconstructed images as shown in Fig. 8. In Fig. 9, the RE value is the smallest and the CC value is almost the largest for the TGV regularization method which further verifies its performance in image reconstruction.

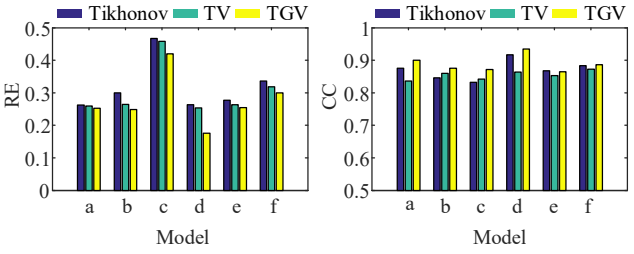

(a) (b)

Fig. 9. The RE and the CC of the reconstructed images with 10% noise level. (a) The RE values. (b) The CC values.

In order to verify the proposed algorithm, a hybrid model with two different edges is also studied, as shown in Fig. 10.

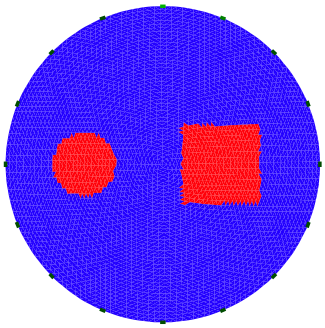

Fig. 10. The hybrid model in which a smooth model and a sharp model exist.

The reconstructed images of the hybrid model with 0%, 5% and 10% noise level added are shown in Fig. 11. It can be seen that the images recovered with the TGV regularization method have clearer edges compared with Tikhonov method and the staircase effect is reduced in comparison to the TV method.

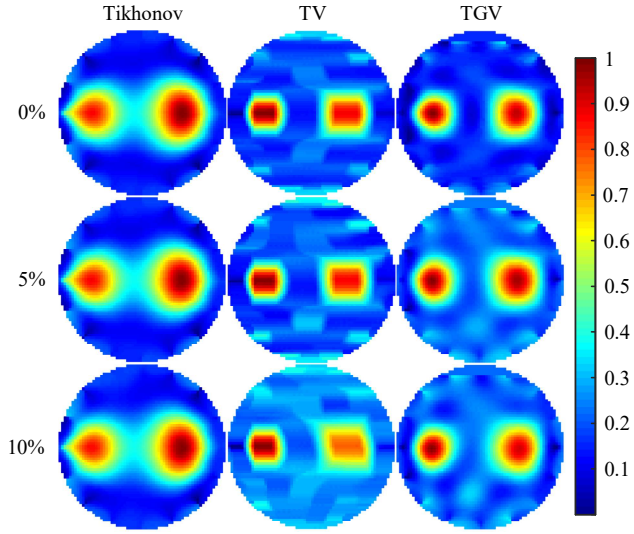

Fig. 11. Reconstructed images of hybrid model under three noise levels

The RE and CC values calculated by the three regularization methods under different noise levels are given in Fig. 12. Compared with the other two methods, the TGV regularization method shows the smallest RE value and the largest CC value at the three noise levels. It ensures the performance of the proposed method in the image reconstruction of hybrid model.

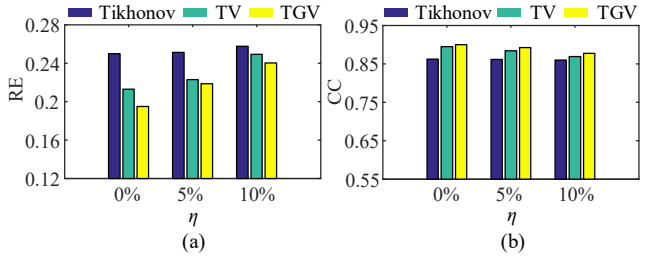

Fig. 12. The RE and the CC of the reconstructed images with different noise level noise level. (a) The RE values. (b) The CC values.

To test the performance of the TGV regularization method when subjected to different levels of noise, the model (a) with smooth edge and model (e) with sharp edge are investigated under the noise level of 0%, 2.5%, 5%, 7.5% and 10%. The related RE and CC values obtained with the three regularization methods are displayed in Fig. 13. It can be seen that the RE values increase while the CC values decreases with the increase of the noise level. In comparison to Tikhonov and TV methods, model (a) with the smooth edge reconstructed by TGV regularization method has the smallest RE values and the largest CC values as shown in Fig. 13(a). For model (e) with the sharp edge, the RE and CC values that are obtained with the TGV regularization method are almost the same with that acquired with TV when the noise level is low, which are better than the Tikhonov method. However, under high noise level, the TGV regularization method shows the smallest RE and nearly largest CC, as depicted in Fig. 13(b).

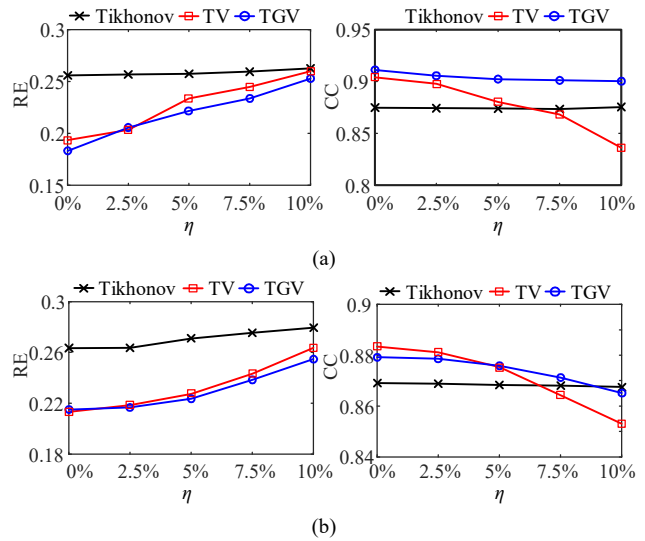

Fig. 13. (a) The RE and CC values for smooth models with different noise level. (b) The RE and CC values for sharp models with different noise level.

B. *Experimental Results*

In this section, static experiments are carried out with the Swisstom Pioneer EIT system in the University of Bath. The experimental results are analyzed to evaluate the feasibility of the proposed TGV regularization method. Sixteen electrodes are installed at equal intervals around the inner side of a cylindrical glass container with the diameter of 14 cm and the height of 25 cm. In the measurement, the adjacent current excitation and the adjacent voltage measurement are adopted. The EIT system works well in the frequency ranging from 45 kHz to 200 kHz. In this work, a lower frequency of 47 kHz is selected as it helps imaging resistivity and not to worry about the permittivity. The current with the amplitude of 1 mA is injected into electrodes of the EIT system. The positions of the objects and the reconstructed images obtained with the Tikhonov, TV and TGV regularization methods are displayed in Fig. 14. As can be seen from Fig. 14, compared with the Tikhonov regularization method, the TV method is preferred for its performance in edge preservation. However, the staircase effect makes it hard to recover both square and circular objects. With the proposed TGV regularization method, the over-smoothness in the Tikhonov method and the staircase effect in the TV method are effectively reduced. It is especially advantageous in reconstructing cross model and hybrid complicated model where smooth turns and sharp turns exist at the same time. It may be a bit challenging when recovering one large and two smaller round objects nearby. Nevertheless, the reconstructed image performs the most excellent among the three regularization methods.

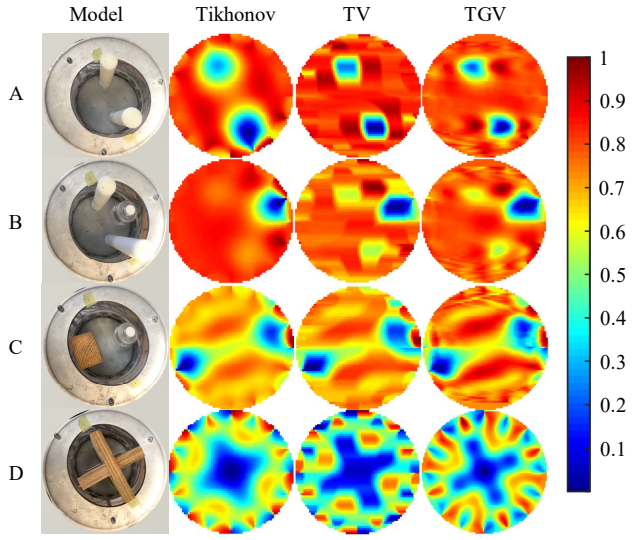

Fig. 14. Reconstructed images based on experimental models.

For a quantitative analysis, the RE and the CC values of the reconstructed images in the experiment are provided in Fig. 15. It can be observed that the TGV regularization method shows the smallest RE values and the largest CC values among the three regularization methods, which validates that the quality of reconstructed images obtained by the TGV regularization method is better than the other two methods.

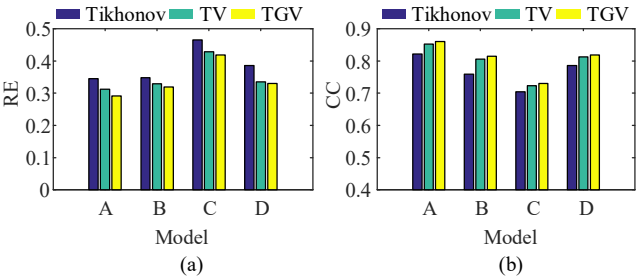

Fig. 15. Comparison of RE and CC values. (a) The RE values. (b) The CC values.

VI. Conclusion

A novel TGV regularization method has been proposed for image reconstruction of EIT. It reduces the staircase effect and preserves the sharp edge in the reconstructed image by combining the first-order and the second-order derivatives as the regularization term. The weight between the two derivatives is adjusted by two weighting factors. Besides, the Chambolle-Pock primal-dual algorithm is applied to solve the proposed regularization method. Simulation and quantitative analysis are performed to investigate the performance of the TGV regularization method. It is found that the proposed TGV regularization method is more superior to the Tikhonov and TV methods in the image reconstruction of models with smooth and with sharp edges, especially when noise is added. It avoids the over-smoothness in the Tikhonov method and reduces the staircase effect in the TV method. In addition, the TGV method also performs well for recovering hybrid complex models. Experiments are also carried out for further validation and the experimental results testify that the proposed TGV regularization method is effective in reducing the staircase effect and the reconstructed images have much higher quality.

Acknowledgments

Yanyan Shi would like to thank the China Scholarship Council for supporting her visit to the University of Bath.

References

[1] B. Y. Sun, S. H. Yue, Z. H. Hao, Z. Q. Cui, and H. X. Wang, "An improved Tikhonov regularization method for lung cancer monitoring using electrical impedance tomography," *IEEE Sens. J.*, vol. 19, no.8, pp. 3049-3057, Apr. 2019.

[2] Z. F. Xu, J. F. Yao, Z. Wang, Y. L. Liu, H. Wang, B. Chen, and H. T. Wu, "Development of a portable electrical impedance tomography system for biomedical applications," *IEEE Sens. J.*, vol. 18, no. 19, pp. 8117-8124, Oct. 2018.

[3] X. T. Shi, W. C. Li, F. S You, X. Y. Huo, C. H. Xu, Z. Y. Ji, R. G. Liu, B. Y. Liu, Y. D. Li, F. Fu, and X. Z. Dong, "High-precision electrical impedance tomography data acquisition system for brain imaging," *IEEE Sens. J.*, vol. 18, no. 14, pp. 5974-5984, Jul. 2018.

[4] Y. Y. Shi, M. Wang, and M. H. Shen, "Characterization of oil-water two-phase flow in a horizontal pipe with multi-electrode conductance sensor," *J. Petrol. Sci. Eng.*, vol. 146, pp. 584-590, Oct. 2016.

[5] S. H. Liu, J. B. Jia, Y. D. Zhang, and Y. J. Yang, "Image reconstruction in electrical impedance tomography based on structure-aware sparse bayesian learning," *IEEE T. Med. Imaging*, vol. 37, no. 9, pp. 2090-2102, Sep. 2018.

[6] S. J. Ren, Y. Wang, G. H. Liang, and F. Dong, "A robust inclusion boundary reconstructor for electrical impedance tomography with geometric constraints," *IEEE T. Instrum. Meas.*, vol. 68, no. 3, pp.762-773, Mar. 2019.

[7] K. Lee, E. J. Woo, and J. K. Seo, "A fidelity-embedded regularization method for robust electrical impedance tomography," *IEEE T. Med. Imaging*, vol. 37, no. 9, pp. 1970-1977, Sep. 2018.

[8] K. Zhang, M. K. Li, F. Yang, S. H. Xu, and A. Abubakar, "Three-dimensional electrical impedance tomography with multiplicative regularization," *IEEE T. Bio-med. Eng.*, Jan. 2019.

[9] E. Dunne, M. O'Halloran, D. Craven, P. Puri, P. Frehill, S. Loughney, S. Loughney, and E. Porter, "Detection of vesicoureteral reflux using electrical impedance tomography," *IEEE T. Bio-med. Eng.*, Dec. 2018.

[10] G. Boverman, D. Isaacson, J. C. Newell, G. J. Saulnier, T. J. Kao, B. C. Amm, X. Wang, D. M. Davenport, D. H. Chong, and R. Sahni, "Efficient simultaneous reconstruction of time-varying images and electrode contact impedances in electrical impedance tomography," *IEEE T. Bio-med. Eng.*, vol. 64, no. 4, pp. 795- 806, Apr. 2017.

[11] Z. F. Xu, J. F. Yao, Z. Wang, Y. L. Liu, H. Wang, B. Chen, and H. T. Wu, "Development of a portable electrical impedance tomography system for biomedical applications," *IEEE Sens. J.*, vol. 18, no. 19, pp. 8117-8124, Oct. 2018.

[12] Z. Wei, D. Liu, and X. D. Chen, "Dominant-current deep learning scheme for electrical impedance tomography," *IEEE T. Bio-med. Eng.*, Jan. 2019.

[13] D. Liu, A. K. Khambampati, and J. F. Du, "A parametric level set method for electrical impedance tomography," *IEEE T. Med. Imaging*, vol. 37, no. 2, pp. 451-460, Feb. 2018.

[14] L. D. Zhou, B. Harrach, and J. K. Seo, "Monotonicity-based electrical impedance tomography for lung imaging," *Inverse Probl.*, vol. 34, no. 4, Apr. 2018.

[15] X. T. Shi, W. C. Li, and F. S. You, "High-precision electrical impedance tomography data acquisition system for brain imaging," *IEEE Sens. J.*, vol. 18, no. 14, pp. 5974-5984, Jul. 2018.

[16] Z. Y. Wang, S. H. Yue, K. Song, X. Y. Liu, and H. X. Wang, "An unsupervised method for evaluating electrical impedance tomography images," *IEEE T. Instrum. Meas.*, vol. 67, no. 12, pp. 2796-2803, Dec. 2018.

[17] S. J. Hamilton, and A. Hauptmann, "Deep d-bar: real-time electrical impedance tomography imaging with deep neural networks," *IEEE T. Med. Imaging*, vol.37, no. 10, pp. 2367-2377, Oct. 2018.

[18] H. Garde, and S. Staboulis, "Convergence and regularization for monotonicity-based shape reconstruction in electrical impedance tomography," *Numer. Math.*, vol. 135, no. 4, pp. 1221-1251, Apr. 2017.

[19] A. K. Khambampati, D. Liu, S. K. Konki, and K. Y. Kim, "An automatic detection of the ROI using otsu thresholding in nonlinear difference EIT Imaging," *IEEE Sensors. J.*, vol. 18, no. 12, pp. 5133-5142, Jun. 2018.

[20] J. Sevcik, V. Smidl, and F. Sroubek, "An adaptive correlated image prior for image restoration problems," *IEEE Signal. Process. Lett.*, vol. 25, no. 7, pp. 1024-1028, Jul. 2018.

[21] X. Li, F. Yang, J. L. Ming, A. Jadoon, and S. Han, "Imaging the corrosion in grounding grid branch with inner-source electrical impedance tomography," *Energies*, vol. 11, no. 7, pp. 1-13, Jul. 2018.

[22] M. S. Gockenbach, and E. Gorgin, "On the convergence of a heuristic parameter choice rule for Tikhonov regularization," *SIAM J. Sci. Comput.*, vol. 40, no. 4, pp. A2694-A2719, 2018.

[23] B. Chen, J. F. P. J. Abascal, and M. Soleimani, "Electrical resistance tomography for visualization of moving objects using a spatiotemporal total variation regularization algorithm," Sensors, vol. 18, no. 6, Jun. 2018.

[24] M. Hinze, B. Kaltenbara, and T. N. T. Quyen, "Identifying conductivity in electrical impedance tomography with total variation regularization," *Numer. Math.*, vol. 138, no. 3, pp. 723-765, Mar. 2018.

[25] J. L. Xu, A. F. Feng, Y. Hao, X. D. Zhang, and Y. Han, "Image deblurring and denoising by an improved variational model," *AEU-Int. J. Electron. C.*, vol. 70, no. 9, pp. 1128-1133, May. 2016.

[26] L. Liu, X. X. Li, K. Xiang, J. Wang, and S. Tan, "Low-dose CBCT reconstruction using Hessian Schatten penalties," *IEEE T. Med. Imaging*, vol. 36, no. 12, pp. 2588-2599, Dec. 2017.

[27] X. W. Liu and L. H. Huang, "A new nonlocal total variation regularization algorithm for image denoising," *Math. Comput. Simulat.*, vol. 97, pp. 224-233, Mar. 2014.

[28] S. H. Wei and G. P. Zhao, "The improvement of total variation based image restoration method and its application," *Math. Methods. Eng.*, pp. 139-151, Jan. 2014.

[29] G. Li, X. Huang, and S. G. Li, "Adaptive Bregmanized total variation model for mixed noise removal," *AEU-Int. J. Electron. C.*, vol. 80, pp. 29-35, Jun. 2017.

[30] K. Bredies, K. Kunisch, and T. Pock, "Total generalized variation," *Siam. J. Imaging. Sci.*, vol. 3, no. 3, pp. 492–526, May. 2010.

[31] B. Xie, C. Xu, Y. Han, and R. K. F. Teng, "Color transfer using adaptive second-Order total generalized variation regularizer," *IEEE Access.*, vol. 6, pp. 6829-6839, Jan. 2018.

[32] X. L. Xu, H. Z. Pan, W. B. Wei, G. D. Wang, and W. Q. Liu, "Multiplicative noise removal based on total generalized variation," *Adv. Image. Graphics. T.*, vol. 757, pp. 43-54, 2018.

[33] S. J. Ren, M. Soleimani, Y. Y. Xu, and F. Dong, "Inclusion boundary reconstruction and sensitivity analysis in electrical impedance tomography," *Inverse Probl. Sci. En.*, vol. 26, no. 7, pp. 1037-1061, 2018.

[34] S. N. Zhang, Y. B. Xu, and F. Dong, "Difference sensitivity matrix constructed for ultrasound modulated electrical resistance tomography," Meas. Sci. Technol., vol. 29, no. 10, Oct. 2018.

[35] H. L. Zhang, L. M. Tang, Z. Fang, C. C. Xiang, and C. Y. Li, "Nonconvex and nonsmooth total generalized variation model for image restoration," *Signal Process*, vol. 143, pp. 69-85, Fed. 2018.

[36] R. H. Chan, H. Liang, S. Wei, M. Nikolova, and X. C. Tai, "High-order total variation regularization approach for axially symmetric object

tomography from a single radiograph," *Inverse. Probl. Imag.*, vol. 9, no. 1, pp. 55-77, Fed. 2015.
[37] J. J. Mei, T. Z. Huang, S. wang, and X. L. Zhao, "Second order total generalized variation for speckle reduction in ultrasound images," *J. Franklin. I.,* vol. 355. no. 1. pp. 574-595, Jan. 2018.
[38] Q. X. Zhong, C. S. Wu, Q. L. Shu, and R. W. Liu, "Spatially adaptive total generalized variation-regularized image deblurring with impulse noise," *J. Electron. Imaging*, vol. 27, no. 5, Sep. 2018.
[39] M. Yan, "A New Primal–Dual algorithm for minimizing the sum of three functions with a linear operator," *J. Sci. Comput.*, vol. 76, no. 3, pp. 1698-1717, Sep. 2018.
[40] G. Schramm, M. Holler, A. Rezaei, K. Vunckx, F. Knoll, K. Bredies, F. Boada, and J. Nuyts, "Evaluation of parallel level sets and Bowsher's method as segmentation-free anatomical priors for time-of-flight PET reconstruction," *IEEE T. Med. Imaging.*, vol. 37, no. 2, pp. 590-603, Feb. 2018.
[41] S. Teniou, M. Meribout, T. AI-Hanaei, F. AI-Zaabi, R. Banihashim, and S. AI-Ghafri, "A new constrained hierarchical reconstruction method for electrical capacitance tomography," *Flow. Meas. Instrum.*, vol. 23, no. 1, pp. 66-75, Mar. 2012.
[42] S. Teniou and M. Meribout, "A new hierarchical reconstruction algorithm for electrical capacitance tomography using a relaxation region-based approach," *Measurement*, vol. 45, no. 4, pp. 683-690, May. 2010.
[43] S. Teniou and M. Meribout, "A multimodal image reconstruction method using ultrasonic waves and electrical resistance tomography," *IEEE Trans. Image Process.*, vol. 24, no. 11, pp. 3512-3521, Nov. 2015.
[44] X. P. Yin, H. C. Wu, J. B. Jia, and Y. J. Yang, "A micro EIT sensor for real-time and non-destructive 3-D cultivated cell imaging," *IEEE Sens. J.*, vol. 18, no. 13, pp. 5402-5412, Jul. 2018.